Lunar crater ejecta distribution and characterization using Mini-RF and LROC-WAC data

Ami J. Desai, Shiv Mohan and Sripada V. S. Murty*

PLANEX, Physical Research Laboratory, Ahmedabad 380 009, India

A detailed quantification of ejecta matter for small craters (<6 km) on the basis of its amount of spatial deposition has been attempted in this study. We used scattering information derived from circular polarization ratio (CPR) and displaying intensity (S_1) from Miniature Radio Frequency (Mini-RF) instrument on-board Lunar Reconnaissance Orbiter (LRO), to characterize the radar backscatter of a large number of craters from Rimae Sirsalis, a highland-mare mixed region for deriving spatial ejecta blanket coverage. The radar derived ejecta blanket extent has been further compared with the amount derived by optical sensor for understanding and assessing the relative merits. In order to accurately estimate the total ejecta deposition, its characterization into finer and coarser material has also been done. We have studied the relation between the measured ejecta extents to the crater geometrical parameters and observed a strong relation between the crater ejecta extent and crater diameter using power or polynomial function.

Keywords: Impact processes, lunar crater, planetary dynamics, radar, spatial ejecta distribution.

IMPACT cratering is a fundamental process responsible for shaping a planetary surface[1,2]. One of the principal characteristics and resultant effect after an impact event is the formation and emplacement of large and small ejecta deposits. For heavily cratered bodies in the solar system, knowledge on the behaviour, amount and distribution of the ejecta generated is essential for the interpretation of local geology as impact ejecta greatly modifies and influences the pre-existing surface in several dramatic ways[3]. Ejecta blankets are important for understanding impact cratering process and can significantly offer important clues on the subsurface properties[4]. An important aspect in lunar surface process, still not fully understood, is quantifying the ejecta as a function of mass and energy of the impactor[5]. The extent and volume of ejecta blanket depends on a number of factors, including the size and mass of the impacting body, surface gravity and atmospheric pressure. In case of the Moon, since surface gravity is less (1.622 ms^{-2}) and there is no atmosphere, the ejecta blanket may extend several times the radius of the central crater in any direction depending on the forces of impacting body, local slopes and topography[6]. Another important aspect which still needs to be understood is estimating the amount of ejecta thickness and its spatial distribution. Since the Moon is devoid of atmospheric and physical, chemical or mechanical weathering, further modification of the lunar surface is only due to impacting and sputtering, where individual micro meteorites and solar wind ions blast a small number of atoms from the rock surface[7]. Apart from this, the process that can appreciably change the pre-existing morphology is a later cratering event in close vicinity to the existing one. Based on information from the available data, a wide range of models and theories have been proposed for measuring the ejecta thickness. Impact events at different scales are capable of modifying millions of square kilometres of lunar surface, excavating deep into the lunar crust and perhaps mantle, spreading enormous volume of ejecta over large areas.

Studies based on the cumulative size frequency distribution of the craters in any region help in determining the age of the surface, which also provides an understanding on the cratering events and resultant surface modifications[8]. With the advent of latest remote sensing techniques capable of providing data at high resolution and precision, it is now possible to characterize the ejecta thickness, its spatial extent as well as its volume over a large surface area[9], quantification of which may provide knowledge on resurfacing processes.

Taking advantage of multiple datasets and on the basis of various lunar and earth cratering studies and the available laboratory cratering experimental data, various models have been put forth for measuring the lunar ejecta thickness[8]. Estimation and assessment on how a discontinuous ejecta blanket lifetime varies with crater diameter has been studied previously using Miniature Radio Frequency instrument (Mini-RF)[10]. Considering similar crater dimensions, studies on analysing and characterizing the gradual change in the morphology of eroding ejecta blankets have also been attempted[11]. Mini-RF on-board Lunar Reconnaissance Orbiter (LRO) spacecraft has revealed a great deal of information related to ejecta distribution, flow, impact melt deposits and their properties, which could not be studied using prior radar data. This is

*For correspondence. (e-mail: murty@prl.res.in)

now been possible to realize through better image quality and resolution. The transitions between radar bright and dark backscatter within a given flow have been attributed to various types of surface roughness changes or through the deposition of rough, blocky material caused by topographic obstructions[12–14].

Earlier, using optical datasets, ejecta variation as well as its thickness studies have been carried out for larger craters, but the same could not be accurately achieved for smaller diameter craters due to sensor limitations. Impact melt flow studies based on optical and microwave data have been carried out for Tycho and Glushko craters[15]. Using radar data it was observed that these craters have large impact melt showing variation in backscatter and circular polarization ratio (CPR) properties. A comparison made with optical data revealed that these variations are observed due to the presence of features such as rafted plates, pressure ridges and ponding within the impact melt flow. The regions show high CPR values, from which it can be inferred that the locations believed to be smooth in optical image might actually be rough regions if studied at centimetre and decimetre scales. Impact melt is also a significant component of the rocks produced by the cratering event. Studies on these measurements indicate that large impact events (which form large craters) produce proportionately larger volumes of impact melt[16], but the available data (both theoretical and geological) are not precise enough and have significant uncertainties in the measurements for detailed estimates.

In this regard, the present study provides an estimate of areal distribution of ejecta extent by direct measurements using a radar system. High-resolution radar imaging helps in discerning detailed information even from small diameter craters, which at a very finer resolution scale is not possible to achieve through optical data because of radar sensitivity to surface roughness even for small diameter craters[3]. Although variation in the ejecta types for small-sized craters can be analysed to some extent using optical imageries, at a much fine resolution it shows saturation as a result of which further accurate classification becomes difficult. Whereas radar sensors, owing to the sensitivity to surface roughness, provide detailed information even at very fine spatial resolutions.

Presently, we have estimated the spatial extent of ejecta blanket from 22 small craters (<6.0 km) using radar data, because of strong dependence of backscatter on surface roughness. We have chosen simple circular craters ranging in diameter from 0.7 to 5.6 km. The craters of this size usually exhibit less complexity in terms of material slumping as well as presence of complex crater morphological features. To understand the usefulness and effectiveness of radar data, a systematic analysis of all the selected craters was also carried out using optical datasets. Radar images with high to medium tone of brightness can be classified as ejecta. CPR has also been examined for its utility in identification and mapping of ejecta deposits[17]. CPR is defined as the ratio of same sense to opposite sense circular polarization. Smooth surfaces will have a low CPR, while rough surfaces will have a high CPR[18]. The Mini-RF instrument on LRO is among the first polarimetric imaging radars outside of the Earth's orbit[19]. Ejecta distribution is also analysed using Mini-RF 'S'-band having 12.6 cm wavelength and 30 m/pixel spatial resolution (zoom mode), which on this scale is highly sensitive to surface roughness, providing detailed information on the ejecta blanket with fine resolution and precision[20]. At this resolution, owing to the sensitivity of the radar for surface roughness, crater ejecta with high to medium backscatter can be easily identified on the images, though poorly distinguished through optical data[11].

Study area and datasets

The present study is focused in the region in and around NE trending Rimae Sirsalis believed to be a lunar graben, which is also the longest rille system on Moon, covering a total distance of more than 400 km in length, less than 4 km wide (average) and 150–230 m deep located at 15.7°S 61.7°W. Located in the highlands south of Grimaldi, it is also the straightest rille on the lunar surface over such a long distance showing little branching and extensions[21,22]. As observed commonly, rilles are most often associated with mare regions, but the geological setting of Rima Sirsalis is unique in a way that it almost entirely crosses the highland region. In the present study, the crater observations are focused surrounding the entire stretch of Rimae Sirsalis. A detailed analysis for 22 craters located within the rille as well as surrounding both sides of the rille has been considered. Locations of the craters with their respective coordinates are shown in Figure 1 and documented in Table 1. This region is specifically a combination of highland and mare types. A detailed investigation on crater analysis and ejecta studies may provide a better understanding on the behaviour of ejecta based on the change in the rock nature. The depth and diameter of a crater will vary on the basis of rock type, which will have an effect on the ejecta expelled. This can be used for a later comparison with ejecta extent from distinct mare and highland regions on the lunar surface for a detailed study.

Multiple remote sensing datasets – LRO Wide Angle Camera (WAC) mosaic images and Mini-RF 'S'-band zoom mode images data and GLD DTM are used. The large datasets collected by various science missions have helped the scientific community to acquire high-resolution images, enabling a thorough analysis from the obtained data[23]. This has further helped in producing high-resolution digital maps and digital terrain models (DTMs). The LRO WAC provides multispectral data images at a scale of 100 m/pixel in seven colour bands over a 60 km swath. The global multispectral imaging helps map important

minerals and to create a global morphology base map[24]. For the present study, LROC WAC mosaic images were used for measuring the crater diameter and extracting information for the estimation of areal ejecta extent.

Mini-RF system is a dual polarized synthetic aperture radar transmitting circular, i.e. left-hand polarization and receiving two coherent orthogonal linear polarizations (H and V)[20]. It is a light-weight synthetic aperture radar (SAR) with two wavelengths operating in the X- and S-bands (4.2 and 12.6 cm respectively) with a spatial resolution of 30 m (zoom mode) and 150 m (baseline mode). The information returned by the radar is represented using the classical Stokes parameters (S1, S2, S3, S4), which are further used to derive information on the radar scattering properties of the lunar surface[4]. Since Mini-RF probes the lunar regolith at two frequencies, it is capable of rendering additional information on the physical properties of the upper metre or two of the lunar surface. Here, in order to understand the scattering properties of ejecta blankets, we have used two products derived from the Stokes parameters CPR and S1. The S1 Stokes polarization parameter images with 12.6 cm (S-band) zoom mode representing the total backscatter cross-section play an important role in identifying the ejecta extent as well distinguishing into fine and coarser material. For any detailed analysis, surface composition and surface topography are important; but the dominant factor affecting the total radar backscatter is roughness on the scale of the wavelength of the radar. So effectively, a 12.6 cm Mini-RF total backscatter image measures the roughness of the surface and near subsurface at scales of centimetres to decimetres, permitting a prominent detection of the spatial deposition of ejecta blankets around craters. Since Mini-RF images have a constant incidence angle of 48°, the sensitivity to ejecta blankets does not vary from image to image, making Mini-RF an ideal tool for such studies[10,25–27].

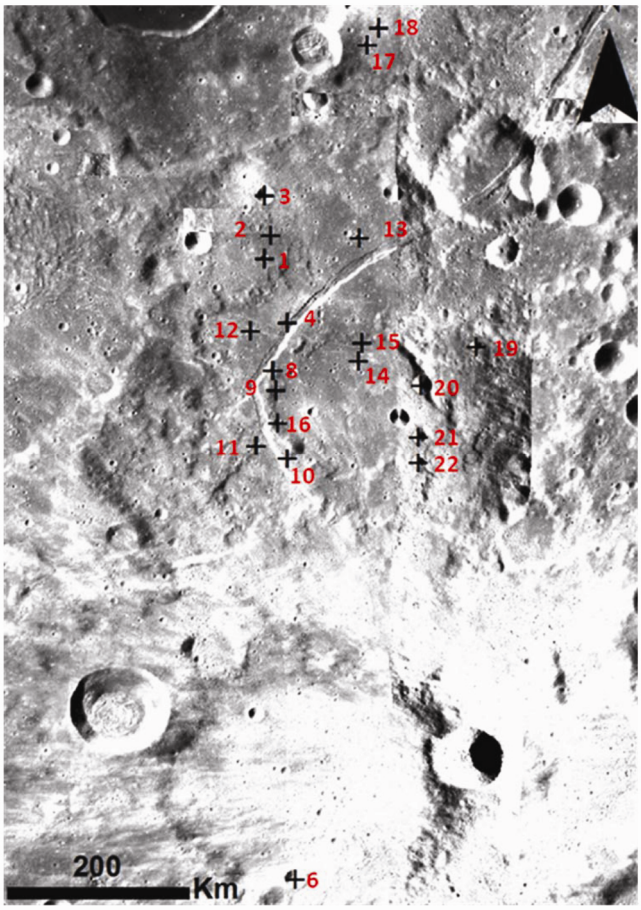

Figure 1. Location of 22 craters selected for the study marked (+) in LROC WAC mosaic image.

For acquiring the depth profile information we used the 'GLD100' data[28]. The WAC DTM is constructed from WAC stereo images and the product we obtain thereby is the global lunar DTM 100 m topographic model, or 'GLD100' covering 98.2% of the lunar surface. Nearly 44,000 LROC WAC stereo images were tied with LOLA for computing GLD100. The GLD100 covers from 79°S to 79°N lat.[28–30]. This combined product has a pixel spacing of 100 m, with vertical accuracy of 10–30 m. It has been further observed that the mean difference between the heights of these two data is only 4 m (ref. 31) and that GLD100 shows less data gaps compared to the limited cross-track coverage of LOLA in the regions away from the poles[32].

Methodology

The required Mini-RF and WAC mosaic images covering the study region were downloaded from the Planetary Data Site (PDS). These were later integrated in ARC-GIS environment and geo-referenced. For understanding the ejecta behaviour with crater diameter, we collected and analysed the depth and diameter of the crater and total spatial extent of ejecta measurements from the selected 22 simple craters ranging in diameter from 0.7 to 5.6 km. Diameter of each crater was obtained from WAC data by taking rim-to-rim dimensions. These were measured by averaging measured diameter at a number of points. Similarly, average depths for each crater were estimated from the depth profile information obtained from GLD100. Since the amount of ejecta expelled after an impact also depends on the excavated crater depth[33], a variation in the depth–diameter to the amount of ejecta expelled is observed.

To understand the variability in measurements of ejecta identification and mapping between optical and microwave data, ejecta extent estimation analysis was done from radar as well as optical images. The LRO Mini-RF utilizes new wideband hybrid polarization architecture to measure Stokes parameters of the reflected signal[27]. Here, in order to calculate the ejecta in terms of its spatial/areal

Table 1. Radar and optically derived ejecta extent and crater parameters for the 22 craters analysed

				Ejecta extent (sq. km) derived using						
				S1			CPR			
Crater no.	Coordinates	Diameter (km)	Depth (m)	Coarse	Fine	Total	Coarse	Fine	Total	Optical total
1	(294.14N, –19.55E)	2.5	40	3.53	8	11.53	6	8.1	14.1	4.96
2	(294.21N, –19.33E)	1.1	2	0.84	1.77	2.61	1.7	3.13	4.83	1.24
3	(294.14N, –20.72E)	5	660	8.86	24.2	33.06	15	21.8	36.8	30.7
4	(294.38N, –20.20E)	1.8	36	1.55	2.56	4.11	2	5	7	3.02
5	(294.44N, –24.53E)	2.5	210	4.71	8.01	12.72	8	8.7	16.7	–
6	(294.50N, –25.62E)	5.9	930	27.8	70	97.8	38	63.4	101.4	–
7	(294.61N, –23.00E)	1.7	90	1.27	5.4	6.67	7	3.45	10.45	–
8	(294.23N, –20.66E)	1.6	9	0.46	4.72	5.18	3	6.68	9.68	3.81
9	(294.26N, –20.88E)	1.6	6	0.53	2.68	3.21	3.5	2	5.5	3.86
10	(294.38N, –21.56E)	1.2	2	0.5	1.72	2.22	1.4	1.7	3.1	2.95
11	(294.06N, –21.42E)	1.4	17	0.89	1.8	2.69	3.33	2.6	5.93	3.34
12	(294.01N, –20.28E)	0.7	2	0.68	1.07	1.75	1.8	2.07	3.87	0.92
13	(295.08N, –19.35E)	2.1	93	3.46	5.73	9.19	5.7	7	12.7	7.17
14	(295.07N, –20.58E)	1.4	16	1.14	1.89	3.03	1.91	4	5.91	2.93
15	(295.11N, –20.40E)	1.3	16	1.56	2	3.56	2.1	2.5	4.6	2.44
16	(294.27N, –21.18E)	2.5	80	0.76	1.2	1.96	5	3	8	9.95
17	(295.16N, –17.38E)	2.4	220	4.91	9.4	14.31	5.1	12.64	17.74	8.41
18	(295.26N, –17.25E)	2.1	215	2.48	11	13.48	6.1	12.1	18.2	9.13
19	(296.24N, –20.37E)	3.5	213	9.23	14	23.23	13.07	13.06	26.13	13.4
20	(295.69N, –20.76E)	5.6	700	18.4	45.6	64	33	35.06	68.06	24.3
21	(295.67N, –21.28E)	4	420	11.5	29.7	41.2	10	34.66	44.66	16.9
22	(295.63N, –21.53E)	4.2	620	13.8	16.9	30.7	14.3	20.1	34.4	19.95

distribution, Stokes parameter 1 (S1), which is the sum of the horizontal and vertical linear polarization channels providing the intensity information has been used. The pixel brightness displays the intensity of the backscattered return[11]. Similar analysis was also done using CPR images because of its higher sensitivity to surface roughness[17], to understand the variability of the ejecta deposition. Similarly, for extracting information from optical data, required craters were mapped and analysed as done for the radar. Further, it was observed that few small-sized craters for which mapping was not possible through optical data, could only be mapped with the aid of radar data (Table 1). Thus it can be said that due to sensitivity of SAR for ejecta and its roughness, it is feasible to derive exact estimate of ejecta spatial extent[34]. Optical data do not provide us information based on similar properties, due to which the information extracted becomes limited.

Several factors contribute to backscatter intensity: the first and most important parameter is the slope of the topography along the look direction. More signal is reflected back when the slope is angled towards the spacecraft. When the slope is angled away from the spacecraft, fewer signals are reflected back. As a consequence, brightened wall is angled towards the spacecraft and the darkened wall is angled away from the spacecraft. Another factor in determining the intensity of the backscatter is the roughness of the surface on the scale of the wavelength of the radar. For instance, the S-band on Mini-RF has a wavelength of 12.6 cm, so it scatters back to the receiver most strongly when the surface it is observing has a large number of decimetre-sized blocks[20]. The transition from bright to dark tone reflects those surfaces that are less blocky or smoother with reference to the wavelength. Fine material represents an increasing fraction of the total ejecta volume with increasing distance from the crater. Thus, ejecta are generally darker as distance increases from the crater[35]. Considering this, the radar response to ejecta was categorized into two tonal variations related to roughness. High backscattering shows a brighter tone and lower backscattering shows a darker tone. The dark ejecta have a value of backscattering coefficient of about –10 dB, whereas bright ejecta are represented by a value of –2.0 dB corresponding to high roughness. Figure 2 shows transect of radar backscatter for different features around the crater. We also analysed the CPR image[25], for which the corresponding measured average values of CPR obtained were 0.36 and 0.03 for bright and dark ejecta respectively. This provides additional information on the roughness characteristics of the surface. Taking this fact into consideration, for deriving accurate information on the total ejecta extent, we have mapped, classified and categorized the ejecta expelled out after an impact as: (1) Coarser ejecta in which the amount of deposition expected is more hummocky or blocky and exhibits a brighter tone due to high backscatter. This type of material is expected to be observed more in close vicinity of the impact due to larger and heavier particle size. (2) Finer ejecta in which the amount of deposition

expected is less and the area covered will be more because of smaller particle size and exhibits a darker tone (Figure 2). The total ejecta deposit extent is estimated by combining both coarser and finer material area mapped using radar brightness values. These variabilities are clearly and easily distinguished based on the radar backscatter variation which is again difficult through optical data, due to which the information from optical data is found to be underestimated. It is seen that a large amount of information is lost in optical data compared to microwave data because of less clarity in terms of tonal variation. In order to understand how the ejecta extent and pattern behave and vary with crater diameter, statistical regression has been carried out.

Results and discussion

The amount of material that is blasted-off by the impactor depends largely on the excavated crater depth. This material which we call ejecta is usually deposited either in a continuous or discontinuous fashion and called ejecta blanket. From our studies also, we observed that the type and spatial distribution of ejecta associated with impacts vary with crater size and depth (Table 1) and the ejecta becomes finer with increasing radial distance. Continuous ejecta blankets around lunar craters are typically blocky and of high albedo, in case of fresh craters[36]. The maximum diameter of boulders in an ejecta blanket increases with crater size[37,38]. Thus, a variable intensity is observed in radar images which basically depend upon the block size (Figure 2). In most of the cases, a clear dichotomy can be observed between the continuous and discontinuous ejecta. Finer matter or more or less discontinuous ejecta is partly observed to get deposited near the cratering site, but largely, most deposition is seen away from the impact site mainly because of the finer particle size which allows it to travel and flow for a far greater distance compared to the coarser materials. Sometimes they also form spectacular long arrays of radiating ejecta pattern often giving rise to ray craters or craters in which ejecta is arranged in a radial pattern[39].

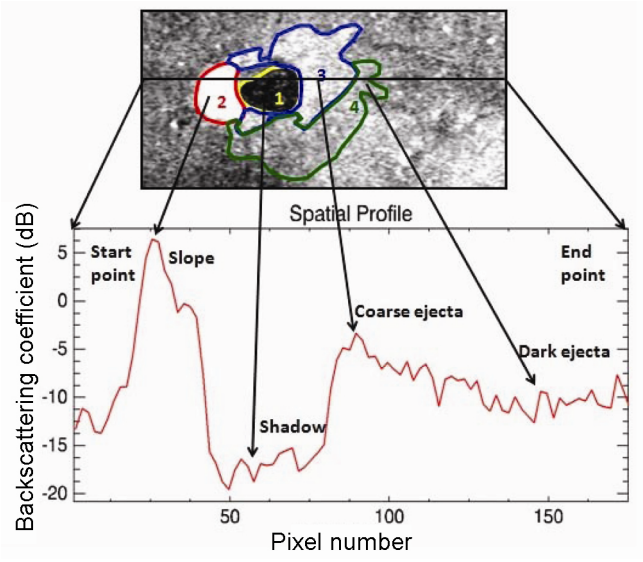

Figure 2. Transect of radar backscattering signal variation along the crater ejecta. The regions with high backscatter are those of coarser surface (rough), whereas regions with comparatively low backscatter are those having finer (smooth) material. The completely dark regions are the areas under shadow. Numbers 1–4 show the regions and type of ejecta material and the corresponding backscattering.

Comparative analysis using optical and radar images

Using optical remote sensing imageries, lunar impact crater materials that are immature or relatively undisturbed and younger are optically bright relative to their surroundings. With time, due to the effect of space weathering in the top few microns of the surface, where optical data are sensitive, such signatures may get subdued. But radar can image these locations due to its longer wavelength. This information can be expressed using derived products such as CPR or S1 images for characterizing ejecta blankets. Mini-RF radar is specifically designed to further differentiate various crater properties[19].

Observations as analysed from optical datasets: As discussed, sensitivity of the radar for ejecta identification is better than the optical sensor. To further strengthen this observation, we have estimated and compared ejecta extent derived from optical and microwave data. Table 1 shows a detailed comparison of impact ejecta extent derived from SAR and WAC data. When the total ejecta estimation obtained by S1 and CPR was analysed, we found that both are almost similar and are thus closely correlated (Figure 3). In addition, we observed that the

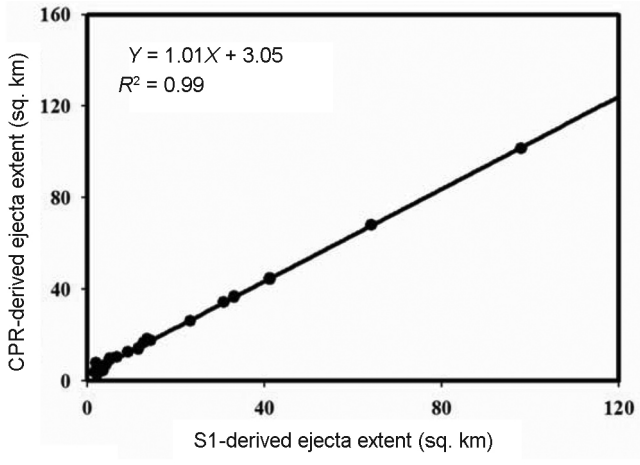

Figure 3. Comparison of total ejecta estimation derived using Mini-RF S1 and CPR images.

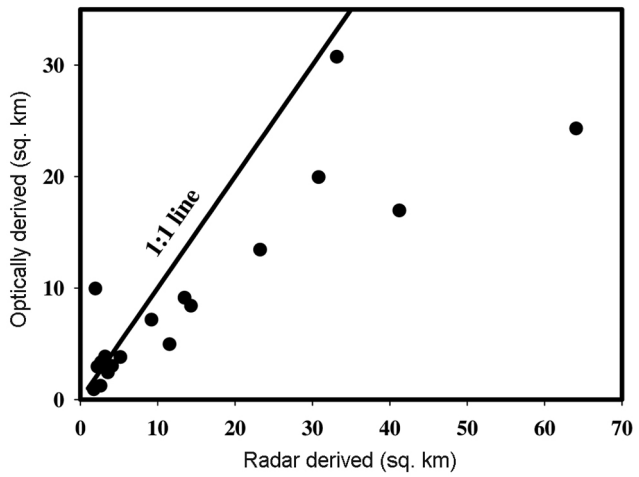

Figure 4. Comparison of ejecta extent derived from S1 radar image and optical datasets for 19 of the 22 craters. Information from optical data is observed to be underestimated compared to radar data.

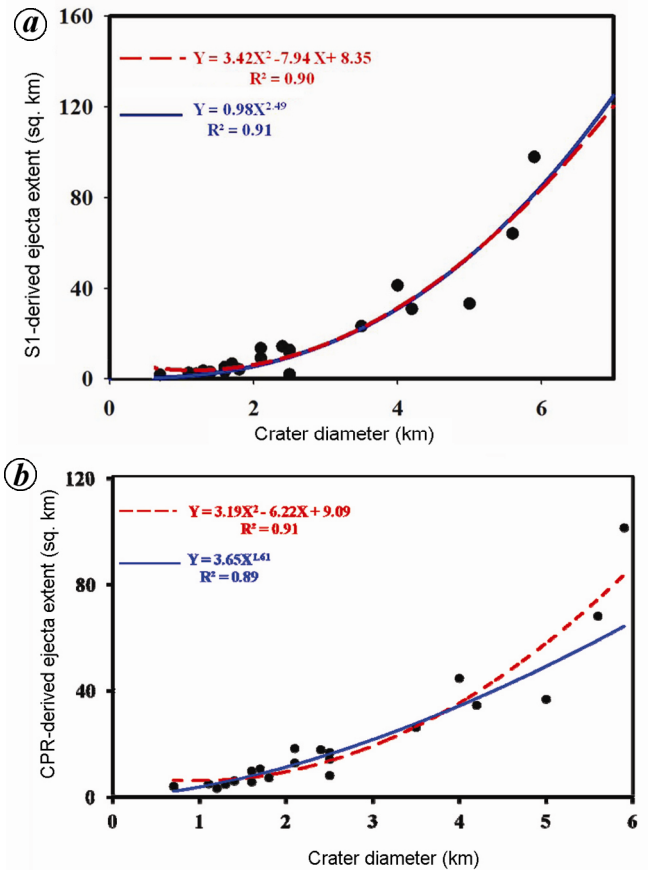

Figure 5. Crater diameter versus radar detected ejecta extent using (***a***) Mini-RF S1 image and (***b***) Mini-RF CPR image. Red dotted line denotes polynomial equation and continuous blue line denotes power derived values.

ejecta extent from almost all the craters was far more clearly discernible from radar data compared to optical counterparts. Only for very small craters falling approximately within a range of 1.5 km, the ejecta extent variation between optical and radar estimates is not much different, as the data fall closer to the 1 : 1 line (Figure 4). But as the crater size increases, the ejecta variation as well as the amount of finer information that can be extracted using radar images start becoming more precise, showing a significant change in the deviation between optical and radar data. This can be attributed to the observed tonal clarity obtained from radar data. Also, we had three craters whose ejecta was not possible to be discerned from optical data, but was easily inferred using radar data (craters 5–7; Table 1). The diameters of these craters are 2.5, 5.9 and 1.7 km respectively. For the remaining 19 craters, it was observed that the ejecta estimation from optical data is greatly underestimated compared to the radar data (Table 1). Optical imageries exhibit an even tone and texture which is not so for the radar data and thus makes it possible to distinguish them better. Also, sensitivity of the radar to surface roughness caused by the ejecta blanket, and its ability to differentiate slope and local topography of the surrounding region play a major role while estimating the total spatial ejecta extent. Figure 4 compares the ejecta extents derived by the optical and radar images.

Observations as analysed from radar datasets: In order to establish and understand the utility of radar-measured crater ejecta extent, we have attempted to relate it with crater diameter. These relations are based on the hypothesis that ejected material dispersed on the lunar surface is proportional to the material excavated from the impact crater. Figure 5 *a* and *b* shows the relationship between crater diameter and ejecta extent derived from both the radar images S1 and CPR respectively. Our observations and analysis on the surface roughness properties which help in identifying and differentiating the types of ejecta showed that CPR and S1 present a similar correlation. The estimated ejecta extent based on S1 and CPR image is highly correlated and shows nearly similar results (Figure 3).

The nature and variation of data shows that there exists a relation of ejecta extent with crater diameter. We have fitted the data by two relations, namely second-order polynomial and power. We used second-order polynomial, since the first-order polynomial is not enough to account for the entire data variation showing a nonlinear pattern. The model relating crater ejecta extent with crater diameter showed very high value of correlation coefficient as 0.90 and 0.91 for S1-derived total ejecta, and 0.91 and 0.89 for CPR-derived total ejecta deposition. The model error for polynomial and power relations in terms of percentage for S1-derived total ejecta estimate is ~7.55 and 7.30 respectively. The ejecta expelled from the craters is not linearly related with crater diameter and a nonlinear relation exists, which can be described by a second-order polynomial or power equation.

Conclusions

Ejecta distribution is one of the important parameter for analysing crater ejecta distribution model on the lunar surface. Presently available theoretical and laboratory experimental data indicates that ejecta from impact events produces proportionately larger volumes of impact ejecta, but the available data (both theoretical and geological) is not precise enough for detailed estimates[40]. The radar data shows distinct signature of ejecta due to its sensitivity to surface roughness. Thus, it is possible to estimate the extent of ejecta using radar brightness measurements. The study brings out the unique application of the radar data for ejecta estimation and its distribution depending on crater dimension. It significantly points to the fact that there exists a direct relation of ejecta expelled to the diameter of the crater. Further, CPR-based measurements or S1 image measurements did not make much difference in the estimate on the extent of ejected material. The analysis indicated that a polynomial and power relation could describe the distribution of ejecta from craters of diameter less than 6 km. The study brings out a new approach for providing data on ejecta extent, distribution and its relation with crater diameter.

1. Werner, S. C. and Medvedev, S., The lunar rayed-crater population – characteristics of the spatial distribution and ray retention. *Earth Planet. Sci. Lett.*, 2010, **295**, 147–158.
2. Patterson, G. W., Cahill, J. T. S. and Bussey, D. B. J., Characterization of lunar crater ejecta deposits using radar data from the Mini-RF instrument on LRO. In 44th Lunar and Planetary Science Conference, The Woodlands, Texas, Abstract #2380, 18–22 March 2013.
3. Wells, K. S. and Bell III, J. F., Characterization of ejecta facies of a small lunar crater in Balmer Basin using LROC data. In 41st Lunar and Planetary Science Conference, The Woodlands, Texas, Abstract #1932, 1–5 March 2010.
4. Patterson, G. W., Stickle, A. M., Bussey, D. B. J., Cahill, J. T. S. and Mini-RF team, Mini-RF observations of the radar scattering properties of young lunar crater ejecta blankets, Houston, Texas, Abstract #2720, 15–19 March 2014.
5. O'Keefe, J. D. and Ahrens, T. J., Impact ejecta on Moon. In Proceedings 7th Lunar Science Conference, 1976, pp. 3007–3025.
6. Hawke, B. R. and Head, J. W., Impact melt on lunar crater rims. In *Impact and Explosion Cratering* (eds Roddy, D. J., Pepin, R. O. and Merrill, R. B.), Pergamon Press, New York, 1977, pp. 815–841.
7. McKay, D. *et al.*, The lunar regolith. In *Lunar Sourcebook: A User's Guide to the Moon* (eds Heiken, G., Vaniman, D. and French, B.), Cambridge University Press, Cambridge, UK, 1991, pp. 285–356.
8. Morota, T. *et al.*, Ejecta thickness of lunar impact basin. In 42nd Lunar and Planetary Science Conference, The Woodlands, Texas, Abstract #1301, 7–11 March 2011.
9. Fassett, C. I., Head, J. W., Smith, D. E., Zuber, M. T. and Neumann, G. A., Thickness of proximal ejecta from the orientale basin from lunar orbiter laser altimeter (LOLA) data: implications for multi-ring basin formation. *Geophys. Res. Lett.*, 2011, **38**, L17201; DOI:10.1029/2011GL048502.
10. Bell, S. W., Thomson, B. J., Dyar, M. D., Neish, C. D., Cahill, J. T. S. and Bussey, D. B. J., Dating small fresh lunar craters with Mini-RF radar observations of ejecta blankets. *J. Geophys. Res.*, 2012, **117**, E00H30; DOI:10.1029/2011JE004007.
11. Bell, S. W., Fresh lunar crater ejecta as revealed by the miniature radio frequency (Mini-RF) instrument on the Lunar Reconnaissance Orbiter, Thesis submitted, Department of Astronomy of Amherst College, Amherst College, 2011, p. 97.
12. Chadwick, D. J. and Schaber, G. G., Impact crater outflows on Venus: morphology and emplacement mechanisms. *J. Geophys. Res. (Planets)*, 1993, **98**(E-11), 20891–20902.
13. Schultz, P. H., Atmospheric effects on ejecta emplacement and crater formation on Venus from Magellan. *J. Geophys. Res.*, 1992, **97**(E10), 16183–16248.
14. Johnson, J. R. and Baker, V. R., Surface property variations in Venusian fluidized ejecta blanket craters. *Icarus*, 1994, **110**(1), 33–70.
15. Carter, L. M., Neish, C. D., Bussey, D. B. J., Spudis P. D., Patterson, G. W., Cahill, J. T. and Raney, R. K., Initial observations of lunar impact melts and ejecta flows with the mini-RF radar. *J. Geophys. Res. Planets*, 2012, **117**(E00H09); DOI: 10.1029/2011JE003911.
16. Grieve, R. A. F. and Cintala, M. J., An analysis of differential impact melt-crater scaling and implications for the terrestrial impact record. *Meteoritics*, 1992, **27**, 526–538.
17. Spudis, P. D., Baloga, S. M., Glaze, L. S., Dixit, V., Pantone, S. M. and Juvanescu, I., Radar scattering and block size properties of lunar crater ejecta from Mini-RF and LROC NAC data. In 43rd Lunar and Planetary Science Conference, The Woodlands, Texas, Abstract #1461, 19–23 March 2012.
18. Cahill, J. T. S., Bussey, D. B. J., Patterson, G. W., Turner, F. S., Lopez, N. R., Raney, R. K. and Neish, C. D., Global Mini-RF S-band CPR and m-Chi decomposition observations of the Moon. In 43rd Lunar and Planetary Science Conference, The Woodlands, Texas, Abstract#2590, 19–23 March 2012.
19. Patterson, G. W., Raney, R. K., Cahill, J. T. S., Bussey, D. B. J., and the Mini-RF Team, Characterization of lunar crater ejecta deposits using m-Chi decompositions of Mini-RF radar data. In EPSC Abstracts, vol. 7, EPSC2012-731, European Planetary Science Congress, 2012.
20. Neish, C. D., Bussey, D. B. J., Spudis, P., Marshall, W., Thompson, B. J., Patterson, G. W. and Carter, L. M., The nature of lunar volatiles as revealed by Mini-RF observations of the LCROSS impact site. *J. Geophys. Res.*, 2011, **116**, E01005; DOI:10.1029/2010JE003647.
21. North, G., *Observing the Moon, The Modern Astronomer's Guide*, Cambridge University Press, 2000, pp. 324–328; 381.
22. Head, J. W., Wilson, L., Anderson, K. A. and Lin, R. P., Lunar linear Rilles, models of dike emplacement and associated magnetization features. In Lunar and Planetary Science Conference XXVIII, Houston, Texas, Abstract#1242, 17–21 March 1997.
23. McEwen, A. S. *et al.*, Mars reconnaissance orbiter's high resolution imaging science experiment (HiRISE). *J. Geophys. Res.*, 2007, **112**, E05S02; DOI:10.1029/2005JE002605.
24. Glaser, P. *et al.*, Improvement of local LOLA DTMs using LROC NAC DTMs – example for an ESA Lunar Lander candidate landing site. In 44th Lunar and Planetary Science Conference, The Woodlands, Texas, Abstract#1967, 18–22 March 2013.
25. Raney, K. R., Hybrid-polarity SAR architecture. *IEEE Trans. Geosci. Remote Sensing*, 2007, **45**, 3397–3404; DOI:10.1109/TGRS.2007.895883.
26. Bussey, D. B. J., Spudis, P. D., Nozette, S., Lichtenberg, C. L., Raney, R. K., Marinelli, W. and Winters, H. L., Mini-RF: imaging radars for exploring the lunar poles. In 39th Lunar and Planetary Science Conference, League City, Texas, Abstract #2389, 10–14 March 2008.
27. Nozette, S. *et al.*, The Lunar Reconnaissance Orbiter miniature radio frequency (Mini-RF) technology demonstration. *Space Sci. Rev.*, 2010, **150**, 285–302; DOI:10.1007/s11214-009-9607-5.

28. Scholten, F., Oberst, J., Matz, K. D., Roatsch, T., Wählisch, M., Robinson, M. S. and LROC team, GLD 100 – the global lunar 100 meter raster DTM from LROC WAC Stereo Models. In 42nd Lunar and Planetary Science Conference, The Woodlands, Texas, Abstract #2046, 7–11 March 2011.
29. Scholten, F., Oberst, J. and Robinson, M. S., GLD100 – lunar topography from LROC WAC stereo. In EPSC Abstracts, EPSC-DPS2011-1272-1, 2011, vol. 6.
30. Scholten, F., Oberst, J., Matz, K. D., Roatsch, T., Wählisch, M., Speyerer, E. J., and Robinson, M. S., GLD100 – the near-global lunar 100 meter raster DTM from LROC WAC stereo image data. *J. Geophys. Res.*, 2012, **117**(E12); DOI:10.1029/2011JE003926.
31. Scholten, F. *et al.*, Complementary Global LRO lunar topography datasets – a comparison of 100 m raster DTMs from LROC WAC stereo (GLD 100) and LOLA altimetry data. In 42nd Lunar and Planetary Science Conference, The Woodlands, Texas, Abstract #2080, 7–11 March 2011.
32. Bray, V. J., Stone, C. A. and McEwen, E. A., Investigating the transition from central peak to peak-ring basins using central feature volume measurements from the global lunar DTM 100 m. *Geophys. Res. Lett.*, 2012, **39**, L21201; DOI:10.1029/2012GL053693.
33. Pike, R. J., Depth/diameter relations of fresh lunar craters: revision from spacecraft data. *Geophys. Res. Lett.*, 1974, **1**(7), 291–294; DOI:10.1029/GL001i007p00291.
34. Cahill, J., Patterson, G. W., Raney, R. K., Bussey, B. and Turtle, E. P., Mini-RF's perspective of the lunar western hemisphere and Orientale Basin's ejecta deposits. In American Geophysical Union, Fall Meeting 2011, Abstract P13G-08, 2011.
35. Ghent, R. R., Campbell, B. A, Hawke, B. R. and Campbell, D. B., Earth-based radar data reveal extended deposits of the Moon's Orientale basin. *Geology*, 2008, **36**, 343–346; DOI:10.1130/G24325A.1.
36. Melosh, H. J., *Impact Cratering: A Geologic Process*, Oxford University Press, New York, 1989, p. 245.
37. Bart, G. D. and Melosh, H. J., Using lunar boulders to distinguish primary from distant secondary impact craters. *Geophys. Res. Lett.*, 2007, **34**; DOI:10.1029/2007GL029306.
38. Osinski, G. R., Tornabene, L. L. and Grieve, R. A. F., Impact ejecta emplacement on terrestrial planets. *Earth Planet. Sci. Lett.*, 2011, **310**, 167–181.
39. Schultz, P. and Lutz, G. A., Grazing impacts on Mars: a record of lost satellites, Part 1. *J. Geophys. Res.* (*Suppl.*), 1982, **87**, A84–A96.
40. French, B. M., *Traces of Catastrophe, A Handbook of Shock – Metamorphic Effects in Terrestrial Meteorite Impact Structures, Impact Melts*, LPI Contribution No 954, Lunar and Planetary Institute, Houston, 1998, pp. 79–90; 120.

ACKNOWLEDGEMENTS. We thank the Department of Space, Government of India for financial support and the two anonymous reviewers for their useful suggestions.

Received 4 April 2014; revised accepted 13 June 2014